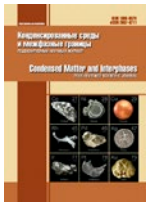

ISSN 1606-867X (Print)
ISSN 2687-0711 (Online)
Condensed Matter and Interphases
Kondensirovannye Sredy i Mezhfaznye Granitsy
https://journals.vsu.ru/kcmf/

Original articles

Research article
https://doi.org/10.17308/kcmf.2024.26/12449

Behavior of major and minor elements during directional crystallization of Fe-Ni-Cu-S-(Rh, Ru, Ir, Pt, Pd, Ag, Au) melt

E. F. Sinyakova✉, **K. A. Kokh**

V. S. Sobolev Institute of Geology and Mineralogy Siberian Branch Russian Academy of Sciences
pr. Akademika Koptyuga 3, Novosibirsk, 630090, Russian Federation

Abstract

The Cu-Fe-Ni-S system is unique in terms of the number of crystalline phases with a variety of combinations of properties, which makes it relevant for prospective material studies. The phases of this system compose typical associations of massive zonal sulfide Cu-Ni ores, and their copper-rich zones are characterized by a high content of noble metals. Therefore, this system is among the most important of those used for the geochemistry of sulfides and for the metallurgy of copper and nickel. There is insufficient quantitative information on the equilibrium distribution coefficients of macrocomponents and the behavior of impurities upon crystallization of solid solutions in the region of the solid-melting diagram corresponding to natural ores or intermediate products of metallurgical production. Therefore, the goal of the work was to obtain new data on the phase diagram of the Cu-Fe-Ni-S system and corresponding phases of noble metals (Rh, Ru, Ir, Pt, Pd, Ag, Au) during the process of fractional crystallization of the melt simulating zonal copper-rich ores of platinum-copper-nickel sulfide deposits.

We conducted quasi-equilibrium directional crystallization of the melt with a composition of (at. %): Fe 29.20, Ni 5.85, Cu 17.60, S 47 with addition of 0.05% of Rh, Ru, Ir, Pt, Pd, Ag, and Au. The obtained sample was studied using optical and scanning electron microscopy, energy-dispersive spectrometry (SEM/EDS), and X-ray phase analysis. Differential thermal analysis (DTA) was used to determine the liquidus temperatures along the crystallization path.

The distribution of macrocomponents along the cylindrical ingot showed that it consisted of five primary zones. Primary phases and phase associations crystallized from the melt in the following sequence: mss / mss + iss / iss / iss + bnss / bnss + pnss, where mss is monosulfide solid solution $(Fe_xNi_{1-x})S_{1\pm y}$, iss is intermediate solid solution $(Cu,Fe)S_{1-x}$, bnss is bornite solid solution $Cu_{5\pm x}Fe_{1\pm x}S_{4\pm y}$, and pnss is pentlandite solid solution $(Fe_xNi_{1-x})_{9\pm y}S_8$. This indicated a complex structure of the solid-melting diagram in the studied region. We determined the crystallization temperatures of mss and iss. A new type of secondary (phase) zoning was identified, formed as a result of subsolidus transformations of primary phases, which can be present in Cu-Ni sulfide ores. It was found that impurities can dissolve in the main sulfide phases, form individual microphases in the sulfide matrix, or be present in these microphases in the form of solid solutions. The main concentrators of Pd were pn and sug. Ir, Rh, and Ru were distributed between mss and pn, and Ag preferred bnss. Most impurities of noble metals formed inclusions as independent microphases: RuS_2, Pt_3Fe, Au* gold-based alloy, Pt-Fe-Au alloy, $CuIr_2S_4$, and native Ag. The results of the work showed that the behavior of macrocomponents could be described using distribution coefficients, and the behavior of microcomponents did not strictly correspond to the classical theory of fractional crystallization of multicomponent melts with impurities.

Keywords: Cu-Fe-Ni-S system, Phase equilibria, Noble metals, Directional crystallization, DTA

Funding: The research was carried out with the financial support of the Ministry of Science and Higher Education of the Russian Federation under the state assignment of the Sobolev Institute of Geology and Mineralogy of the Siberian Branch of the Russian Academy of Sciences No. 122041400237-8 and No. 122041400031-2.

Acknowledgements: Powder X-ray diffraction, scanning electron microscopy, energy-dispersive spectrometry (SEM/EDS) studies were performed at the Centre for Collective Use of multi-element and isotope studies of the Siberian Branch of the Russian Academy of Sciences.

✉ Elena F. Sinyakova, e-mail: efsin@igm.nsc.ru

For citation: Sinyakova E. F., Kokh K. A. Behavior of major and minor elements during directional crystallization of Fe-Ni-Cu-S-(Rh, Ru, Ir, Pt, Pd, Ag, Au) melt. *Condensed Matter and Interphases*. 2024;26(4): 755–771. https://doi.org/10.17308/kcmf.2024.26/12449

Для цитирования: Синякова Е. Ф., Кох К. А. Поведение основных элементов и примесей при направленной кристаллизации расплава Fe-Ni-Cu-S-(Rh, Ru, Ir, Pt, Pd, Ag, Au). *Конденсированные среды и межфазные границы*. 2024;26(4): 755–771. https://doi.org/10.17308/kcmf.2024.26/12449

1. Introduction

The Cu-Fe-Ni-S system is unique in terms of the number of crystalline phases with a variety of combinations of properties, which makes it relevant for prospective material studies. Therefore, this system is among the most important of those used for the geochemistry of sulfides and for the metallurgy of copper and nickel [1-10]. From a geochemical point of view, the most interesting region of this system is located in the vicinity of the iron monosulfide (Fe,Ni)$S_{1\pm\delta}$ (mss) composition. There is only one paper dedicated to the construction of a quantitative model of a fragment of the phase diagram of the Cu-Fe-Ni-S system [3]. The authors obtained equations for the liquidus and solidus surfaces in the iron-rich mss crystallization region with an S content of 50 to 52.5 at. % and also approximated the data for the distribution coefficients of nickel, iron, and copper during its crystallization from the melt. It is obvious that this region should be expanded and a similar description should be obtained for other solid solutions, as well as for regions of multiphase crystallization.

So far, many fragments of the phase diagram of this system and its subsystems Cu-Fe-S and Fe-Ni-S have been characterized by discrepancies between the results of studies by different authors, and these differences were found not only in quantitative data, but also in the fundamental features of the structure of the phase diagrams. The problems of immiscibility of the quaternary melt of the Cu-Fe-Ni-S system [5, 6], mechanisms of formation of the intermediate solid solution (Cu,Fe)S_{1-x}, $CuFe_2S_3$ cubanite, $(Fe,Ni)_9S_8$ pentlandite, $CuFeS_2$ chalcopyrite and the boundaries of their regions of existence in the temperature-composition coordinates [11–16] are still a matter of debate. For example, in [3] the existence of two intermediate solid solutions was assumed: $Cu_{1+x}Fe_{1+x}S_2$, iss, stable up to 900-950 °C in nickel-poor compositions, and a new (Fe,Cu,Ni)S quaternary solid solution between iss and mss that exists at temperatures below 850 °C. There is not enough quantitative information on the positions of the conodes (i.e. on the equilibrium distribution coefficients of the components) upon crystallization of solid solutions in a wide range of temperature and melt composition variations in the middle part of the melting diagram near 50 at. % S.

This system has been widely used to model the formation of magmatic platinum-bearing copper-nickel deposits. Massive ore bodies of these deposits are characterized by highly expressed chemical and mineral zoning. Copper-poor zones are enriched in Ir, Os, Ru, and Rh, while copper-rich zones are enriched in Pd, Pt, Au, Ag, and chalcophile elements (Te, As, Bi, Sb and Sn) [5, 7, 17–22]. Zoning is associated with the hypothesis of the origin of ore bodies as a result of fractional crystallization of sulfide melt [5, 7, 17, 20, 21, 23–26]. For experimental modeling of this process we carried out the quasi-equilibrium directional crystallization of melts simulating natural sulfide melts [27–30]. The prospects for using directional crystallization in the study of phase diagrams of sulfide systems are mainly related to the possibility of determining the equilibrium compositions of the melt and solid phases at an arbitrary moment of crystallization. Theoretical analysis and experiments on directional crystallization of sulfide melt showed the possibility of the existence of several types of zoning, which are determined by the composition of the initial melt and the structure of the phase diagram of the Cu-Fe-Ni-S system and its boundary systems: Cu-Fe-S and Fe-Ni-S [31]. Due to the complexity of the analysis of fractional crystallization of natural Cu-Ni sulfide melts and the lack of information for theoretical modeling, direct experimental studies of the Cu-Fe-Ni-S-(noble metals) model system are of interest for sulfide copper-nickel ores and intermediate products of metallurgical production. Therefore, the goal of the work was to obtain new data on the phase diagram of the Cu-Fe-Ni-S system and on the types of formation of noble metals during the process of fractional crystallization of the melt simulating copper-rich zonal sulfide platinum-copper-nickel ores.

2. Experimental

A sample of the initial composition (at. %): Fe – 29.20, Ni – 5.85, Cu – 17.16, S – 47.00, Rh, Ru, Ir, Pt, Pd, Au, Ag, 0.05 of each was obtained from pure metals (99.99%) and analytically pure sulfur (99.99%) by heating the mixture of elements in a quartz ampoule evacuated to a residual pressure of $1.5 \cdot 10^{-2}$ mm Hg to 1000 °C. It was held at this temperature for 24 hours and then cooled in air. The synthesized sample with a weight of about 11 g was placed in a quartz ampoule with a conical bottom, which was evacuated to $1.5 \cdot 10^{-2}$ mm Hg. Crystallization was performed by the Bridgman-Stockbarger method in a two-zone furnace with a diaphragm. The container with the sample was placed in the upper zone of the furnace, heated until the sample melted, and held for two days. Then it was lowered into the cold zone at a speed of $2.25 \cdot 10^{-8}$ m/s. This regime provided quasi-equilibrium conditions for directional crystallization. In this case, the obtained results can be attributed to the phase diagram of the Cu–Fe–Ni–S system. The temperature at the lower end of the quartz ampoule was 890 and 601 °C at the beginning and end of crystallization, respectively. Once crystallization was complete, the ampoule was cooled in the switched-off furnace.

The resulting ingot, approximately 120 mm long and 8 mm in diameter, was cut perpendicular to the longitudinal axis into 25 pieces. They were weighed and the fraction of crystallized melt g was determined. Fifteen fragments were used to prepare and study the polished sections. We identified a list of phases and their chemical composition in each fragment. The average chemical composition of the ingot, as well as the average composition of inclusions and local composition of phases were measured at the Analytical Center for Multielement and Isotope research, Siberian Branch of the Russian Academy of Sciences (using energy-dispersive spectrometry (SEM-EDS) on a MIRA 3 LMU high-resolution microscope (Tescan Orsay Holding) equipped with INCA Energy 450+ X-Max 80 and INCA Wave 500 (Oxford Instruments Nanoanalysis Ltd) microanalysis systems. The K series (S, Fe, Cu, Ni) and L series (Rh, Ru, Ir, Pt, Pd, Au, Ag) of X-ray radiation were used for the analysis. FeS_2 (on S) and pure Fe, Ni, Cu, Rh, Ru, Ir, Pt, Pd, Au, Ag were used as references. The measurements were performed at an accelerating voltage of 20 kV, an electron beam current of 1.5 nA, and a live spectra accumulation time of 30 s. With these analytical conditions, the lower limit of the detectable concentrations was 0.4–0.5 wt. % for Pt, Au, and Ir and 0.1–0.2 wt. % for the remaining elements. The error did not exceed 1–1.5 rel. % in determining the main components and 2–5 rel. % for impurities. To estimate the average composition of multiphase sections, we used the total spectrum obtained by scanning sections with an area of up to 1.5 mm^2. To reduce the lower limit of detectable concentrations by approximately twice, we increased the the accumulation time of spectra up to 120 s. The average composition of phase mixtures was calculated from 3–5 analyses from different sections of each cross-section along the ingot. The error in determining the main components was 1–2 rel. %.

The melt composition at an arbitrary moment of crystallization was calculated from the average chemical composition of the solid phases using the material balance equation [32]:

$$c_i^L = \frac{c_{i0} - \int_0^g c_i^S dg}{1-g}.$$

Here g is the mole fraction of the crystallized melt ($g = 0$ corresponds to the melted sample, while $g = 1$ corresponds to the solidified sample), c_{i0} is the concentration of the i-th component in the initial ingot, c_i^s is the average concentration of the i-th component in the ingot layer of thickness dg adjacent to the crystallization front, c_i^L is the average concentration of the i-th component in the melt.

The phases were diagnosed by powder X-ray diffraction on a DRON-4 automated powder diffractometer using CuK_α radiation with a graphite monochromator. The diffraction patterns were scanned in the range of 2θ to 8° up to 90° with a step of 0.05°, and the scanning time per point was 4 s, with a slit of 0.5 mm. The obtained diffraction patterns were decoded using the ASTM database. The parameters were calculated using the UnitCell program. The sample from the initial zone was recorded with an external standard of Si.

Differential thermal analysis (DTA) was performed for three specially synthesized samples with compositions located along the

crystallization path. To perform DTA, we placed a sample weighing ~ 50 mg in a thermoanalytical cell in the form of an evacuated quartz ampoule with a concave bottom, which was installed on the thermocouple junction. The melting temperatures of the samples were determined by the reference-free DTA method with heating at a rate of 10 deg/min. The thermocouple was tested using the melting point of gold (1063 °C). The error in recording the temperature was ± 5 °C.

Table 1 contains a list of the phases obtained during the experiment and their designations.

3. Results and discussion

3.1. Behavior of macrocomponents

Based on the data on the change in the chemical composition of the substance along the ingot (Table 2), we plotted the distribution curves of the components up to g = 0.86 (Fig. 1). The trajectory of the melt composition upon crystallization is also presented, and the values of the average distribution coefficients of components between the solid ingot and the melt are provided. The average chemical composition of the substance of the ingot zones and the average distribution coefficients of macrocomponents changed abruptly when moving from one zone to an adjacent one. These data indicated that the resulting ingot consisted of five primary zones. Fig. 1 shows the process in a simplified way, although it clearly demonstrates the general patterns of crystallization of a zonal sample.

In zone I ($0 \leqslant g \leqslant 0.28$), the average chemical composition of the ingot changes from $Fe_{40.19}Ni_{6.16}Cu_{2.08}S_{50.86}Ru_{0.38}Rh_{0.15}Ir_{0.20}$ to $Fe_{38.85}Ni_{7.76}Cu_{2.17}S_{51.07}Ru_{0.08}Rh_{0.01}Ir_{0.07}$. It can be seen that upon crystallization Fe and Ni generally transited into solid solutions (κ_{Fe} = 1.4–1.5,

Table 1. Phases obtained in the present work in the Cu-Fe-Ni-S-(Pt, Pd, Rh, Ru, Ir, Au,Ag) system Intermediate solid solution

Phase	Designation	Formula
Primary solid solutions (ss) crystallizing from the melt		
Monosulfide ss	mss	$(Fe_xNi_{1-x})S_{1\pm y}$
Intermediate ss	iss	$(Cu,Fe)S_{1-x}$
Bornite ss	bnss	$Cu_{5\pm x}Fe_{1\pm x}S_{4\pm y}$
Pentlandite ss	pnss	$(Fe_xNi_{1-x})_{9\pm y}S_8$
Secondary phases formed as a result of Subsolidus transformations during cooling of the sample		
Monosulfide ss	mss’	$(Fe_xNi_{1-x})S_{1\pm y}$ (Ni from 6 to 10 at.%)
Ni-rich Monosulfide ss	Ni-mss	$(Fe_xNi_{1-x})S_{1\pm y}$ (Ni ~19 at. %)
Low-temperature intermediate ss of haycockite composition	iss’	$(Cu,Fe)S_{1-x}$ (Fe > Cu) $Cu_4Fe_5S_8$
Low-temperature intermediate ss of mooihoekite composition	iss’	$(Cu,Fe)S_{1-x}$ (Fe = Cu) Cu9Fe9S16
Pentlandite	pn	$(Fe, Ni)_9S_8$ (at. ratio Fe/Ni = 1)
Fe-rich Pentlandite	Fe-pn	$(Ni, Fe)_9S_8$ (at. ratio Fe/Ni = 1.1-1.3)
Ni-rich Pentlandite	Ni-pn	$(Ni, Fe)_9S_8$ (at. ratio Fe/Ni = 0.90-0.96)
Sugakiite	sug	$Cu(Fe,Ni)_8S_8$ (Fe/Ni ~ 1-1.5), Cu to 7 ат.%)
Bornite	bnss’	$Cu_{5\pm x}Fe_{1\pm x}S_{4\pm y}$
Native copper	Cu	Cu
Фазы благородных металлов		
Laurite	RuS_2	RuS_2
Isoferroplatinum	Pt_3Fe	Pt_3Fe
Gold-based alloy	Au*	Au from 52 to 69 at. %, impurities Ag, Cu, Pd
Alloy of Pt-Fe-Au system	Pt-Fe-Au	Pt-Fe-Au
Native silver	Ag	Ag
Cuproiridsite	$CuIr_2S_4$	$(Cu,Fe)(Ir,Rh,Pt)_2S_4$

Table 2. Average concentrations of elements in the ingot and in the melt

g	Average solid composition, at. %					Melt composition, at. %				
	Fe	Ni	Cu	S	Rh	Fe	Ni	Cu	S	Rh
Zone I (0 ⩽ g ⩽ 0.28)										
0.04	40.19	6.16	2.08	50.86	0.15	28.74	5.84	18.25	46.84	0.05
0.09	40.13	6.38	2.15	50.79	0.14	28.09	5.81	19.17	46.61	0.04
0.25	38.85	7.76	2.17	51.07	0.01	25.79	5.39	22.80	45.66	0.05
Zone II (0.28 ⩽ g ⩽ 0.40)										
0.28	36.71	8.5	4.35	50.45	<mdl	25.35	5.26	23.55	45.47	0.05
0.33	34.47	8.17	7.82	49.54	<mdl	24.56	5.01	24.90	45.12	0.05
Zone III (0.40⩽ g ⩽ 0.68)										
0.40	26.64	4.59	22.39	46.37	<mdl	24.34	5.06	25.17	44.98	0.06
0.49	25.87	4.98	23.02	46.13	<mdl	24.08	5.07	25.54	44.78	0.07
0.57	24.78	5.17	24.51	45.54	<mdl	23.94	5.05	25.74	44.64	0.08
Zone IV (0.68 ⩽ g ⩽ 0.89)										
0.68	19.56	4.27	33.05	43.05	0.07	25.55	5.34	23.05	45.21	0.11
0.79	19.37	4.34	33.07	43.12	0.10	28.61	5.83	18.07	46.22	0.17
0.86	19.04	4.46	33.24	43.07	0.10	33.82	6.57	9.77	47.91	0.26
Zone V (0.89 ⩽ g ⩽ 1)										
0.89	19.86	9.49	25.55	44.06	0.11	–				
0.92	20.07	9.66	24.29	44.67	0.12	–				
0.94	20.08	9.70	24.22	44.66	0.12	–				

Note. mdl – minimum level of elements determination by SEM/EDS method.
In zone I the content of Ru in solid 0.08–0.38 at. %, in melt 0.01–0.04 at. %.
Ir in solid 0.07–0.20 at. %, in melt 0.03–0.04 at. %, in zones II–IV the content of these elements <mdl.
In zone V the content of Au about 0.15 at. %, Pt about 0.37 at. %, Pd up to 0.40 at. %, Ag about 0.30 at. %; in zones I–IV the content of these elements <mdl.

κ_{Ni} = 1.0-1.4), while Cu was rejected to melt (κ_{Cu} = 0.1). Sulfur has a weak tendency to concentrate in the solid ingot (κS = 1.1).

In zone II (0.28 ⩽ g ⩽ 0.40), the composition of the ingot is $Fe_{36.7\text{-}34.5}Ni_{8.5\text{-}8.2}Cu_{4.4\text{-}7.8}S_{50.4\text{-}49.5}$. Since the distribution coefficients were $\kappa > 1$ for Fe and Ni, these components generally transited into the solid phase. Copper accumulated in the melt during crystallization (κ_{Cu} = 0.2–0.3). The sulfur distribution coefficient was κ_S = 1.1.

In zone III (0.40 ⩽ g ⩽ 0.68), the composition of the ingot is $Fe_{26.6\text{-}24.8}Ni_{4.6\text{-}5.2}Cu_{22.4\text{-}24.5}S_{46.4\text{-}45.5}$. The distribution coefficients of the components between the solid phase and the sulfide melt were close to 1. This signifies a minor modification to the composition of the solid phase that was released from the melt. Since κ_{Fe} = 1.09–1.02 and κ_S = 1.03, it was slightly enriched with these components, and since κ_{Cu} = 0.9, it indicated that the sulfide melt was slightly enriched with Cu. The distribution coefficient of nickel (κ_{Ni}) changed from 0.9 at the beginning of this zone to 1 at its end.

In zone IV (0.68 ⩽ *g* ⩽ 0.86), the average composition $Fe_{19.31\pm0.25}Ni_{4.35\pm0.10}Cu_{33.11\pm0.12}S_{43.07\pm0.06}$ solidified from the melt. Upon crystallization, the solid phase was enriched with copper (κ_{Cu} = 1.4–3.4), while the sulfide melt was enriched with the remaining components (κ_{Ni} = 0.7–0.8, κ_{Fe} = 0.6–0.8, κ_S ~ 0.9).

As for zone V (0.86 ⩽ *g* ⩽ ~1), Fig. 1 shows only the average composition of the ingot. Its abrupt change in relation to zone IV and the differences in microstructure and association of secondary phases (Fig. 2) allowed assuming the existence of a new zone at the end of the ingot.

Fig. 2 shows a scheme of a directionally crystallized sample and the microstructure of its cross sections. Studies of the polished sections also showed that the ingot consisted of five zones. When passing from one zone to another, the microstructure of the samples changed abruptly. Structural elements in the form of large grains and lamellae consisting of one or several phases can be identified in the micrographs of the samples. It can be assumed that some

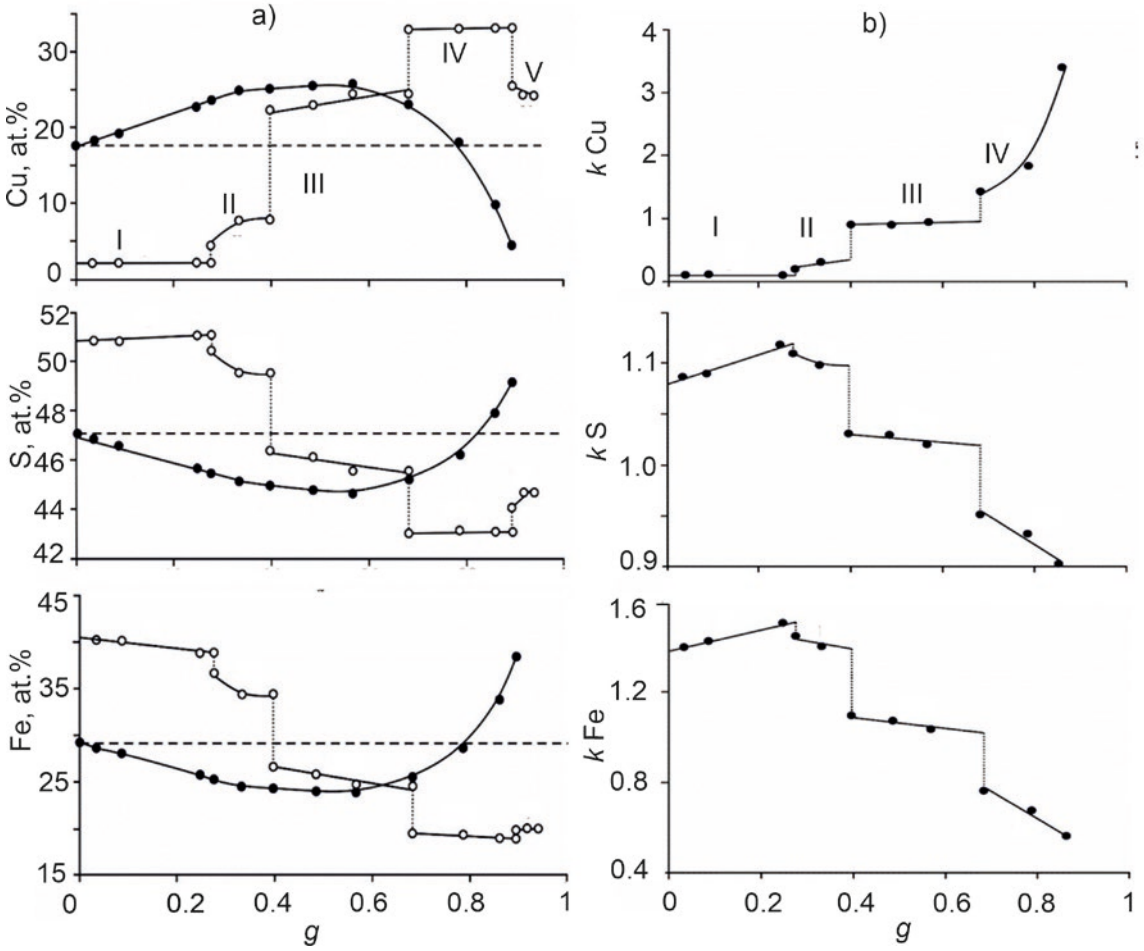

Fig. 1. Change in the average concentration of Cu, S, and Fe in the sulfide melt (closed circles) and solid ingot (open circles) up to *g* 0.85 (a) and the dependence of the average distribution coefficients of these components between solid ingot and melt on *g* (b). The dashed horizontal line shows the concentration of the component in the initial melt, the dashed vertical lines separate the zones

multiphase formations appeared as a result of the solid solution decay initially formed from the melt. Determination of their average chemical composition taking into account the existing data on high-temperature phases in the Cu-Fe-Ni-S system and its boundaries Cu-Fe-S and Fe-Ni-S systems allowed identifying these primary phases and reconstructing the primary phase zoning of the sample (Table 3). Local analysis allowed recording the phase composition of the sample corresponding to the temperature range in which phase reactions ceased upon cooling. The expected temperatures are ~ 300–400 °C. The results of the study of the phase composition of the ingot related to ~ "isothermal" sections of the phase diagram in this temperature range (Table 4).

During the first stage, an iron-rich solid solution containing about 2 at. % Cu and 6–8 at. % Ni, which is usually called monosulfide (mss), crystallized from the melt. In the Fe-Ni-S system, there is a wide mss region between high-temperature FeS_{1+x} and NiS_{1+x} [1, 4]. It is known that up to 8 at. % of copper can be dissolved in it [33]. The initial section of the trajectory of the change in the melt composition was in the region of primary crystallization of this solid solution. According to DTA, the liquidus temperature was 956 °C at the beginning of mss crystallization and 902 °C at the point of the end of its crystallization.

The microstructure of the sample cooled to room temperature consisted of a matrix of low-temperature monosulfide solid solution mss' and rare inclusions of intermediate solid solution iss' of a composition close to haycockite ($Cu_4Fe_5S_8$, hc) (Table 4, Fig. 2c, g = 0.09). It was found that mss' had a hexagonal unit cell with parameters a = 6.8890±0.0070 Å, c = 40.0995±0.0872 Å, unit with

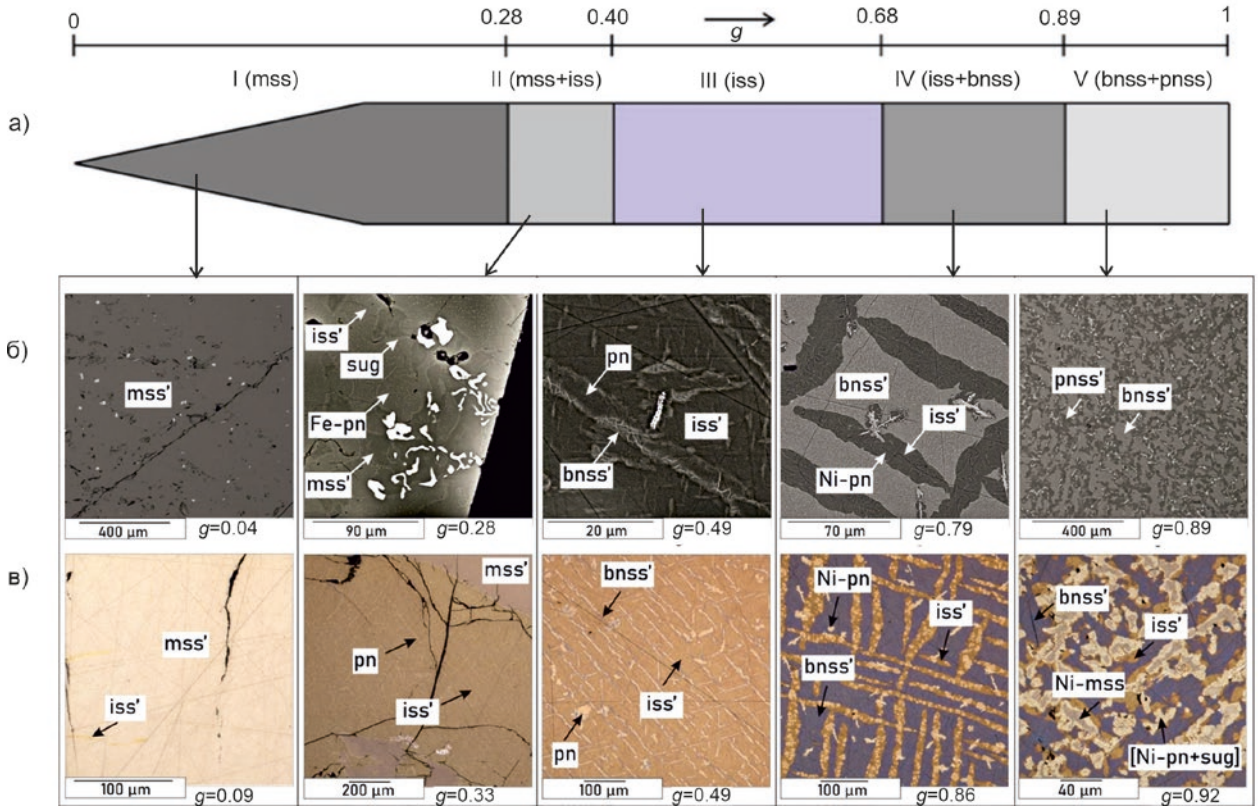

Fig. 2. Schematic of the directionally crystallized sample showing the primary zones (I-V) (a) and the characteristic microstructure of secondary phases in reflected electrons (b) and reflected light (c). See text for comments and phase designations

cell volume 1648.0809 ± 3.1008 Å^3. The release of hc was associated with a decreased copper solubility in mss when the sample was cooled to room temperature.

Upon transitioning from zone I to zone II, the sample underwent an abrupt enrichment with copper and depletion of sulfur (Fig. 1). The micrographs (Fig. 2b, c, g = 0.28, 0.33) showed large inclusions in the mss' matrix, representing a finely dispersed decomposition structures, with average composition $Fe_{28.78\pm0.11}Ni_{4.44\pm0.11}Cu_{19.22\pm0.18}S_{47.58\pm0.39}$, corresponding to the intermediate solid solution iss (Table 3). The amount of iss gradually increased along zone II. These data allowed us to conclude that the change in the composition of the sample was mainly caused by the appearance of iss. The Ni-containing intermediate solid solution is known to coexist with the melt in the Cu-Fe-Ni-S system [29, 30]. This allowed us to assume that the Ni-containing solution in our experiment was also formed in the process of crystallization from a sulfide melt at a temperature of 902 °C of a two-phase cotectic (mss + iss). Upon further cooling, iss decomposed into several phases that formed a characteristic decomposition structure of iron-rich iss' (atomic ratio Fe/Cu ~ 1.5), iron-rich pentlandite Fe-pn (atomic ratio Fe/Ni ~ 1.2) in the form of grains and rims at the boundary of mss' and iss', and Cu(Fe,Ni)8S8 sugakiite (Table 4, Fig. 2b, c, g = 0.28, 0.33). It should be noted that the iss matrix also contained finely dispersed inclusions sized < 1 μm that could not be identified.

In zone III, the average chemical composition $Fe_{25.76\pm0.93}Ni_{4.1\pm0.30}Cu_{23.31\pm1.09}S_{46.01\pm0.43}$ corresponded to an intermediate iss solid solution. This means that the trajectory of the melt composition from the cotectic surface proceeded into the field of primary crystallization of iss. The crystallization path associated with such a transition was described in [31]. The microstructure of zone III consisted of iss' (hc), bornite solid solution (bnss'), and iron-rich pentlandite (Fe-pn) (Fig. 2b, c, g = 0.49, Table 4).

The transition from zone III to zone IV led to an abrupt increase in the copper content

Table 3: Average composition of primary phases along the ingot and partition coefficients of components between these phases and the sulfide melt

g	Phase	Composition of phases, at. %									*k* (Solid/L)			
		Fe	Ni	Cu	S	Ru	Rh	Pd	Ag	Ir	Fe	Ni	Cu	S
Zone I mss (0 ⩽ g ⩽ 0.28)														
0.04	mss	40.19	6.16	2.08	50.86	0.38	0.15	< mdl	< mdl	0.2	1.40	1.05	0.11	1.09
0.09	mss	40.13	6.38	2.15	50.79	0.28	0.14	< mdl	< mdl	0.13	1.43	1.10	0.11	1.09
0.25	mss	38.85	7.76	2.17	51.07	0.08	<0.01	< mdl	< mdl	0.07	1.51	1.44	0.10	1.12
Zone II mss + iss (0.28 ⩽ g ⩽ 0.40)														
0.28	mss	38.1	8.99	2.19	50.73	< mdl	< mdl	< mdl	< mdl	< mdl	1.50	1.71	0.09	1.12
	iss	28.85	4.52	19.34	47.3	< mdl	< mdl	< mdl	< mdl	< mdl	1.14	0.86	0.82	1.04
0.33	mss	37.61	9.51	1.98	50.90	< mdl	< mdl	< mdl	< mdl	< mdl	1.53	1.90	0.08	1.13
	iss	28.7	4.36	19.09	47.85	< mdl	< mdl	< mdl	< mdl	< mdl	1.17	0.87	0.77	1.06
Zone III iss (0.40 ⩽ g ⩽ 0.68)														
0.40	iss	26.64	4.59	22.39	46.37	< mdl	< mdl	< mdl	< mdl	< mdl	1.09	0.91	0.89	1.03
0.49	iss	25.87	4.98	23.02	46.13	< mdl	< mdl	< mdl	< mdl	< mdl	1.07	0.98	0.90	1.03
0.57	iss	24.78	5.17	24.51	45.54	< mdl	< mdl	< mdl	< mdl	< mdl	1.02	1.02	0.95	1.02
Zone IV iss + bnss (0.68⩽ g ⩽ 0.89)														
0.68	iss	28.43	1.47	23.86	46.24	< mdl	< mdl	< mdl	< mdl	< mdl	1.11	0.28	1.03	1.02
	bnss	13.72	0.27	45.37	40.63	< mdl	< mdl	< mdl	< mdl	< mdl	0.54	0.05	1.97	0.90
0.79	iss	28.03	1.81	23.62	46.54	< mdl	< mdl	< mdl	< mdl	< mdl	0.49	0.07	2.48	0.88
	bnss	14.02	0.42	44.75	40.82	< mdl	< mdl	< mdl	< mdl	< mdl	0.98	0.31	1.31	1.01
0.86	iss	27.63	4.81	20.78	46.78	< mdl	< mdl	< mdl	< mdl	< mdl	0.82	0.73	2.13	0.98
	bnss	13.78	0.22	45.71	40.29	< mdl	< mdl	< mdl	< mdl	< mdl	0.41	0.03	4.68	0.84
Zone V bnss + pnss (0.89⩽ g ⩽ 1)														
0.89	bnss	13.99	0.30	44.13	41.25	< mdl	< mdl	< mdl	0.33	< mdl	–	–	–	–
	pnss	24.02	24.94	3.47	46.55	< mdl	0.24	0.78	< mdl	< mdl	–	–	–	–
0.92	bnss	14.04	0.23	44.36	41.21	< mdl	< mdl	< mdl	0.16	< mdl	–	–	–	–
	pnss	24.25	23.69	2.79	47.79	< mdl	0.58	0.53	< mdl	0.36	–	–	–	–
0.94	bnss	13.96	0.41	43.18	41.63	< mdl	< mdl	< mdl	0.82	< mdl	–	–	–	–
	pnss	23.28	25.67	2.36	46.92	< mdl	0.45	1.06	< mdl	0.27	–	–	–	–

Note. mdl – minimum level of element determination by SEM/EDS method. In zone I partition coefficients (mss/L): *k* Ru =10.48, 12.56 and 6.92, *k* Ir = 4.57, 3.35, 1.96 at *g* = 0.04, 0.09 and 0.25, respectively; *k* Rh = 3.27 and 3.46 at *g* = 0.04 and 0.09, respectively

Table 4. Composition of secondary phases in zones along the ingot

g	Phase	Sum, wt. %	Composition, at. %								
			Fe	Ni	Cu	S	Ru	Rh	Pd	Ag	Ir
1	2	3	4	5	6	7	8	9	10	11	12
Zone I (0 ⩽ g ⩽ 0.28) mss' + iss'(hc)											
0.04	mss'	99.45	40.19	6.16	2.08	50.86	0.38	0.15	< mdl	< mdl	0.20
	iss' (hc)	98.45	28.80	0.87	20.11	50.23	< mdl	< mdl	< mdl	< mdl	< mdl
0.09	mss'	99.67	40.13	6.38	2.15	50.79	0.28	0.14	< mdl	< mdl	0.13
	iss' (hc)	99.16	30.00	1.85	20.01	48.14	< mdl	< mdl	< mdl	< mdl	< mdl
0.25	mss'	99.93	38.85	7.76	2.17	51.07	0.08	0.01	< mdl	< mdl	0.07
	iss' (hc)	Not defined									
Zone II (0.28 ⩽ g ⩽ 0.40) mss' + iss'(hc) + Fe-pn +sug											
0.28	mss'	101.04	37.3	10.08	2.07	50.46	< mdl	< mdl	< mdl	< mdl	< mdl
	iss' (hc)	100.76	30.30	1.26	19.69	48.76	< mdl	< mdl	< mdl	< mdl	< mdl
	Fe-pn	100.81	28.55	22.73	1.57	47.01	< mdl	< mdl	0.15	< mdl	< mdl
	sug	101.08	28.35	19.27	4.84	47.39	< mdl	< mdl	0.14	< mdl	< mdl

Eng of Table 4

1	2	3	4	5	6	7	8	9	10	11	12
0.33	mss'	99.06	37.81	9.60	2.33	50.25	< mdl	< mdl	< mdl	< mdl	< mdl
	iss' (hc)	98.89	28.57	0.84	23.26	47.33	< mdl	< mdl	< mdl	< mdl	< mdl
	Fe-pn	99.08	26.05	25.18	1.44	46.89	< mdl	< mdl	0.44	< mdl	< mdl
	sug	Not defined									
0.40	mss'	98.52	36.47	10.22	3.64	49.50	< mdl	0.15	< mdl	< mdl	< mdl
	iss' (hc)	98.01	27.76	1.82	23.82	46.59	< mdl	< mdl	< mdl	< mdl	< mdl
	Fe-pn	97.77	27.40	22.87	2.37	47.0	< mdl	< mdl	0.36	< mdl	< mdl
	sug	98.47	26.75	19.28	7.44	46.28	< mdl	< mdl	0.13	< mdl	< mdl
Zone III (0.40 ⩽ g ⩽ 0.69) iss' (hc) + pn + bnss'											
0.48	iss' (hc)	99.08	27.54	0.79	25.21	46.46	< mdl	< mdl	< mdl	< mdl	< mdl
	pn	99.07	25.24	25.88	1.74	46.81	< mdl	< mdl	0.33	< mdl	< mdl
	bnss'	101.97	15.59	0.4	43.26	40.75	< mdl	< mdl	< mdl	< mdl	< mdl
0.57	iss' (hc)	98.95	27.17	3.11	23.41	46.31	< mdl	< mdl	< mdl	< mdl	< mdl
	pn	Not defined									
	bnss'	101.26	13.75	0.30	45.95	40.00	< mdl	< mdl	< mdl	< mdl	< mdl
Zone IV (0.68⩽ g ⩽ 0.89) iss'(hc) + Ni-pn + bnss' +Cu											
0.68	iss' (hc)	99.36	27.86	0.83	24.71	46.61	< mdl	< mdl	< mdl	< mdl	< mdl
	Ni-pn	99.95	25.2	25.68	1.78	46.88	< mdl	< mdl	0.46	< mdl	< mdl
	bnss'	100.22	13.72	0.27	45.37	40.63	< mdl	< mdl	< mdl	< mdl	< mdl
	Cu	97.75	1.06	0.28	98.34	0.32	< mdl	< mdl	< mdl	< mdl	< mdl
0.79	iss' (hc)	98.67	28.17	1.21	23.78	46.84	< mdl	< mdl	< mdl	< mdl	< mdl
	Ni-pn	100.27	24.78	25.82	1.88	47.06	< mdl	< mdl	0.45	< mdl	< mdl
	bnss'	100.67	14.02	0.42	44.75	40.82	< mdl	< mdl	< mdl	< mdl	< mdl
	Cu	99.18	2.34	0.39	96.91	0.36	< mdl	< mdl	< mdl	< mdl	< mdl
0.86	iss' (hc)	100.98	28.82	1.34	21.72	48.12	< mdl	< mdl	< mdl	< mdl	< mdl
	Ni-pn	101.18	24.71	26.29	1.84	46.69	< mdl	< mdl	0.47	< mdl	< mdl
	bnss'	100.79	13.78	0.22	45.71	40.29	< mdl	< mdl	< mdl	< mdl	< mdl
	Cu	Not defined									
Zone V (0.89 ⩽ g ⩽ 1) iss' (mh) + Ni-pn + sug + Ni-mss + bnss'											
0.89	iss' (mh)	101.12	26.33	0.9	25.75	47.03	< mdl	< mdl	< mdl	< mdl	< mdl
	Ni-pn	102.07	23.02	25.84	2.78	46.57	< mdl	0.22	1.56	< mdl	< mdl
	sug	101.47	24.49	22.75	4.76	47.09	< mdl	0.14	0.77	< mdl	< mdl
	Ni-mss	101.57	28.26	18.35	1.79	50.03	< mdl	0.71	< mdl	< mdl	0.58
	bnss'	101.82	13.57	0.28	44.68	40.89	< mdl	< mdl	< mdl	0.59	< mdl
0.92	iss'(mh)	98.12	25.14	1.02	26.40	47.44	< mdl	< mdl	< mdl	< mdl	< mdl
	Ni-pn	100.08	23.33	25.77	1.93	46.97	< mdl	< mdl	2.0	< mdl	< mdl
	sug	100.3	25.43	20.15	5.06	48.68	< mdl	0.36	< mdl	< mdl	0.32
	Ni-mss	99.73	27.40	18.64	1.81	50.82	< mdl	0.75	< mdl	< mdl	0.57
	bnss'	100.44	14.04	0.23	44.36	41.21	< mdl	< mdl	< mdl	0.16	< mdl
0.94	iss'(mh)	Not defined									
	Ni-pn	103.93	23.28	25.67	2.36	46.92	< mdl	0.45	1.06	< mdl	0.27
	sug	103.23	24.93	21.33	4.54	48.16	< mdl	0.48	0.19	< mdl	0.38
	Ni-mss	Not defined									
	bnss'	102.60	13.67	0.32	44.6	41.13	< mdl	< mdl	< mdl	< mdl	< mdl

Note. Au and Pt content in all phases < mdl. mss' – low-temperature monosulfide solid solution (Ni 6-10 at. %), Ni-mss – nickel monosulfide solid solution (Ni~19 at. %), iss' – low-temperature intermediate solid solution, bnss' – low-temperature boronitic solid solution (Ni 6-10 at. %), iss' – low-temperature intermediate solid solution, bnss' – low-temperature bornite solid solution, Fe-pn – pentlandite with Fe/Ni = 1.1-1.3, pn – pentlandite with Fe/Ni=1, Ni-pn – pentlandite with Fe/Ni=0.90-0.96, sug – sugakiite $Cu(Fe,Ni)_8S_8$, Cu – native copper.

and a decrease in the iron and sulfur content in the sample (Fig. 1). Large lamellar inclusions, representing a finely dispersed decay structure, were visible in the micrographs (Fig. 2b, c, g = 0.79, 0.86). They have an average composition of $Fe_{27.6\text{-}28.4}Ni_{1.5\text{-}4.8}Cu_{20.8\text{-}23.9}S_{46.2\text{-}46.8}$, so they should be attributed to the intermediate solid solution (iss). These inclusions were present in the matrix of the bornite solid solution $Fe_{13.7}Cu_{45.4}Ni_{0.3}S_{40.6}$ (bnss) (Table 3). The obtained data allowed stating that the change in the sample composition was mainly caused by the appearance of bnss in it. In [34, 35] it was shown that in the middle part of the phase diagram of the Cu-Fe-S system, the liquidus surface consisted of the fields of primary crystallization of the pyrrhotite solid solution (poss), the digenite-bornite solid solution Cu_2S–Cu_5FeS_4 (bnss), and the intermediate solid solution $CuFeS_2$–$Cu_3Fe_4S_6$ (iss). The ternary eutectic poss + bnss + iss, as well as quasi-binary eutectics (poss + bnss), (poss + iss), and (iss + bnss) were present on the liquidus surface. Bnss is also known to coexist with the melt in the Cu-Fe-Ni-S system [28]. Thus, in our experiment, the melt trajectory can also correspond to the crystallization of the cotectic (iss + bnss). We found that iss decomposed upon cooling to form low-temperature iss' of the $Fe_{27.6\text{-}28.2}Ni_{1.21\text{-}4.8}Cu_{20.8\text{-}24.7}S_{46.6\text{-}46.8}$ composition, Ni-pn with an atomic ratio of Fe/Ni = 0.96-1, while bnss decomposed into low-temperature bnss' and native copper (Fig. 2b, c, g = 0.79, 0.86, Table 4).

It was difficult to determine the exact set of primary phases released from the melt in zone V due to its complex structure. The decomposition was complicated by the formation of intergrowths of sulfide minerals with impurity phases, the amount of which took up a noticeable fraction of this section of the sample (Fig. 2b, c, g = 0.89, 0.92). It is possible that during the transition from zone IV to zone V, the trajectory of the melt composition entered the crystallization region of the bivariant cotectic of pnss ($Fe_{23.3\text{-}24.2}Ni_{23.4\text{-}25.7}Cu_{2.4\text{-}3.5}S_{46.6\text{-}47.8}$) + bnss ($Fe_{14.0}Ni_{0.2\text{-}0.4}Cu_{43.2\text{-}44.4}S_{41.2\text{-}41.6}$) (Table 3, Fig. 2b, g = 0.89, 0.92). It should be noted that previously we obtained the bivariant cotectic (bnss + pnss) in [28]. The following low-temperature phases were present in zone V: iss' of mooihoekite composition (mh), Ni-pn, Ni-mss, sug and bnss' (Table 4, Fig. 2c, g = 0.92) and, possibly, other unidentified phases of basic sulfides.

3.2. Behavior of microcomponents

Over the course of the directional crystallization of the sulfide melt, impurities can pass into the solid ingot either in the main phases as solid solutions or form inclusions as independent phases (e.g., [16, 28]). Let us study the behavior of noble metals in the experiment.

3.2.1. Solid solution in base metal sulfides

Noble elements in primary sulfide solid solutions. The results on the mss composition in zone I presented in Table 3 showed that Ir, Ru, and Rh were concentrated in this phase at the initial moment of melt crystallization. Their distribution coefficients mss/L > 1, which was consistent with the data in [6, 22, 36–38]. The content of Pt, Pd, Ag, and Au in mss was less than the minimum level of their detection by SEM/EDS. However, their content measured by the precision laser ablation method allowed calculating the distribution coefficients mss/L: k Pt 0.02-0.2, k Pd <0.03-0.2, k Au 0.01-0.09 [6, 14, 36–39]. According to the data in [22], the values of k for Pd, Pt, Au, and Ag ranged from ~ 0.1 to ~ $1 \cdot 10^{-3}$, so these elements should be mainly expelled into the melt.

The content of noble metals in primary mss, iss, and bnss in zones II-IV was below the limit of their detection by SEM/EDS (Table 3). Therefore, these crystallization stages were accompanied by a more intense accumulation of impurities in the melt. According to [22], the distribution coefficients of Pt, Pd, Ag, and Au had low values, which led to the enrichment of the sulfide liquid with these elements. Pt and Au were not found in iss [14, 40], Rh dissolved in sulfur-rich iss [41], while Pd (up to 0.4 at.%) could enter into iss with Cu > Fe and into Ni-rich iss (up to 1 at.%) [14]. Data on the directional crystallization of sulfide melts showed that 0.13-0.15 at. % Au could dissolve in iss with Cu > Fe [42]. Bornite solid solution associated with Ni-rich iss could dissolve 0.1 at. % Pd [14].

Measurement of the average composition of the ingot in zone V showed that the bnss + pnss cotectic crystallized in it. According to the data in Table 3, Pd and Rh were concentrated in pnss (0.8 and 0.2 at. %, respectively), and Ag expelled into bnss (0.3 at. %), which corresponded to the results obtained earlier in [28].

Noble elements in secondary sulfide solid solutions. In zone I, up to 0.15 at. % Rh can be dissolved in low-temperature mss' (Table 4). In zone II, the content of impurities of all noble metals in mss' was less than the analytical error. Upon cooling, iss decomposed into a mixture of iss', Fe-pn, and sug. The Pd was distributed between Fe-pn and sug. Obviously, Pd was initially present in iss, which was crystallized from the melt in this zone. In zone III, up to 0.3 at. % Pd could be dissolved in pn with the atomic ratio Ni / Fe = 1. The main concentrator of Pd in zone IV was Ni-pn. In zone V, Pd and Rh were distributed between Ni-pn and sug. Rh can also be present in Ni-mss.

3.2.2. Phases of micro-elements

The sample contained phases that were synthetic analogues of the following minerals: RuS_2 laurite, $Pt_{3-x}Fe$ isoferroplatinum, $CuIr_2S_4$ cuproiridsite, as well as an alloy based on native gold Au*, native silver Ag, and a solid solution of the composition Pt-Fe-Au.

RuS_2. At the beginning of the crystallization process (g ~ 0.04), a mass formation of laurite RuS_2 was observed (Fig. 3a). Laurite was present in the mss' matrix as single faceted crystals sized about 15 μm^2 and plates sized about 3 x 30 μm or their fragments (Fig. 3 a-c). It may contain the following impurities (at.%): 0.9-4.7 Ir, about 0.5 Rh, 0.4 Pd, 0.2 Ag, up to 1.7 Fe, and 0.4 Ni (Table 5). The heterogeneity of the chemical composition of the laurite crystals should be noted: their central zone was richer in ruthenium, and the edge zone was doped with iridium, which was consistent with the data in [43].

Ruthenium remaining in the melt was released in zones IV and V as large rare single crystals of RuS_2 sized up to 130 μm^2 (Fig. 3 n, j, k) and in intergrowths with $CuIr_2S_4$ cuproiridsite (Fig. 3 k, n). The Ir impurity in laurite varied from ~5 to ~8 at. %, and RuS_2 may also contain Rh, Pd, Ag, Ni, Fe, and Cu (up to 0.5-1 at. %).

$CuIr_2S_4$. Iridium formed its own phase, similar in composition to the natural mineral of the thiospinel group – $CuIr_2S_4$ cuproiridsite. $CuIr_2S_4$ was present in zones IV and V in the form of isolated inclusions of irregular shape sized about 20 μm^2 and in intergrowths with RuS_2 sized up to 150 μm^2 (Fig. 3 k, l, m). Cuproiridsite contained up to 2 at. % of Pt and Rh, about 5 at. % Fe and ~4 at. % Ni (Table 5).

Pt_3Fe. Platinum formed a phase similar to the mineral isoferroplatinum Pt_3Fe. It was detected in the mss' matrix in zones I and II as dendritic structures of inclusions ranging in size from ⩽ 1 μm to about 7 x 15 μm (Fig. 3g, zone I; Fig. 3e, zone II). Isoferroplatinum contained about 1 at. % Au, about 3 at. % Cu and Ni (Table 5).

For the analysis of gold-based alloy Au*, solid solution of Pt-Fe-Au composition, and native Ag, we selected the largest inclusions, but they are usually smaller in size than the value of the X-ray generation zone, i.e. up to about 1 μm. Therefore, the results of the analysis of the composition of these phases were contaminated with components of the host phase.

Au*. Gold formed an independent phase containing (at.%): from ~ 53 to ~ 69 Au and impurities of Pd (up to 10 at.%), Ag (up to 6 at.%) and Pt (up to 1.5 at.%) (Table 5). These impurities formed solid solutions with Au, which was consistent with the structure of the solid-melting diagrams of binary Au-Ag, Au-Cu, Au-Pd and ternary systems Au-Ag-Cu and Au-Ag-Pd [44, 45]. Au* inclusions were localized in zone II in the iss' matrix and in zone V at the mh / Ni-pn interphase boundaries as elongated inclusions about 1 μm wide and 10–30 μm long (Fig. 3e, 3p)

Pt-Fe-Au solid solutions. The Pt-Fe-Au microphase was established in zones II–V. In zones II and III, the results of the analysis of the composition of this solid solution were strongly contaminated with the components of the pentlandite matrix. In zones IV and V, its composition varied within the following range (at. %): Pt from 43.2 to 49.0, Fe from 21.7 to 23.7, Au from 7.4 to 14.9 (Table 5). This phase was present in the form of isolated inclusions or colonies of inclusions of a maximum size of up to 5 μm long and up to 1–2 μm wide in the matrix Fe-pn in zone II (Fig. 3g), pn in zone III (Fig. 3h), Ni-pn in zone IV (Fig. 3k, m) and Ni-mss in zone V (Fig. 3n, o, p). The high content of Pt, Fe, and Au and the nature of decomposition similar to that in similar inclusions in [28] allowed attributing the discovered inclusions to a Pt-Fe-Au solid solution. The authors of [28] found that in case of cooling, inclusions of such a solid solution decomposed into a mixture of $Pt_{3-x}Fe$ and an alloy based on Au*.

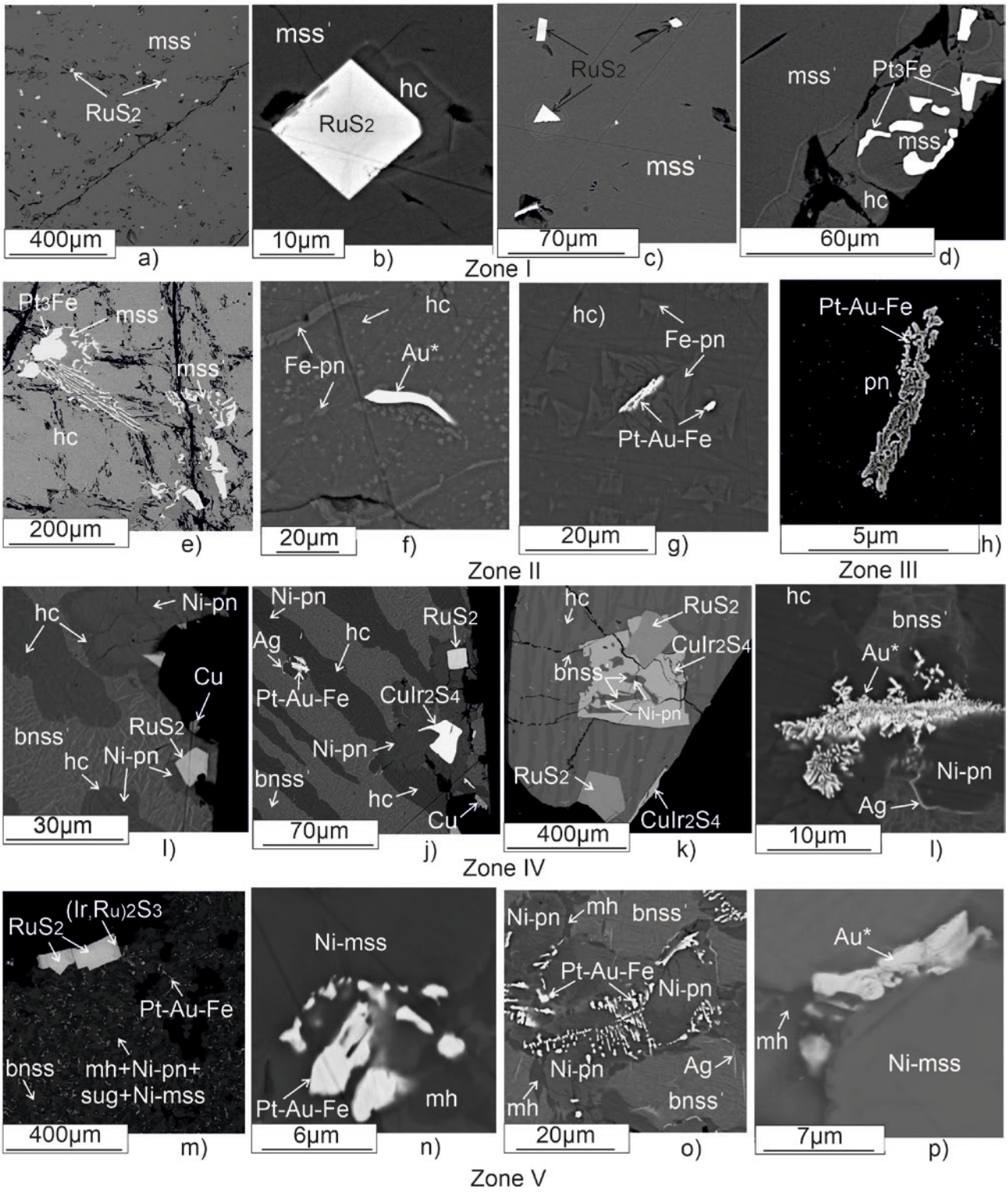

Fig. 3. Forms of noble metal microphase separation in sulfide matrices in zones I–V. Microphotographs were obtained in reflected electrons. RuS_2 crystals in the mss' matrix at g 0.04 (a, b, c); Pt_3Fe inclusions in the mss' matrix at g 0.09 (d) and 0.33 (e); Au* inclusions in the hc' matrix at *g* 0.28 (f) and in the Ni-mss' matrix at *g* 0.92 (p); single RuS_2 and $CuIr_2S_4$ inclusions in Ni-pn matrix at *g* 0.68 (i, j); RuS_2 and $CuIr_2S_4$ intergrowths at *g* 0.86 (l) and 0.92 (n); Pt-Fe-Au alloy inclusions in pn at *g* =0.57 (h), in Ni-pn at *g* 0.68 (k), 0.86 (m) and 0.92 (n, o, p)

Table 5. Chemical composition of selected grains of characteristic microphases of noble metals in the sample

Phase	Ideal formula	Fe	Ni	Cu	Au	Ag	Pt	Pd	Ru	Ir	Rh	S	Сумма
Zone I (mss)													
Laurite	RuS_2	1.23	0.27	–	–	0.46	–	–	56.04	3.1	0.82	36.13	98.05
		1.27	0.26	–	–	0.25	–	–	31.93	0.93	0.46	64.9	
		1.19	0.29	–	–	0.44	–	0.77	54.79	6.98	–	37	101.46
		1.2	0.28	–	–	0.23	–	0.41	30.63	2.05	–	65.2	
		1.63	0.42	–	–	–	–	–	46.77	15.37	–	35.47	99.65
		1.73	0.42	–	–	–	–	–	27.46	4.74	–	65.64	
Isoferroplatinum	Pt_3Fe	11.01	1.02	1.08	1.48	–	81.32	–	–	–	–	0.42	96.33
		29.47	2.6	2.54	1.12	–	62.31	–	–	–	–	1.96	
Zone II (mss+iss)													
Isoferroplatinum	Pt_3Fe	11.8	1.35	1.36	–	–	84.09	–	–	–	–	0.45	99.06
		30.15	3.28	3.05	–	–	61.51	–	–	–	–	2	
Gold-based alloy	Au*[1]	2.33	0.85	5.36	85.82	0.86	–	2.51	–	–	–	0.76	98.48
		6.61	2.29	13.36	68.99	1.26	–	3.74	–	–	–	3.75	
Alloy of Pt-Fe-Au system	Pt-Fe-Au[1]	11.76	7.35	6.83	42.42	1.85	17.07	4.01	–	–	–	10.96	102.26
		18.43	10.96	9.4	18.84	1.5	7.66	3.3	–	–	–	29.91	
Zone III (iss)													
Alloy of Pt-Fe-Au system	Pt-Fe-Au[1]	13.29	9.51	8.28	36.65	1.88	17.49	3.81	–	–	–	13.2	104.11
		18.72	12.75	10.25	14.64	1.37	7.05	2.82	–	–	–	32.39	
Zone IV (iss+bnss)													
Native silver	Ag[1]	18.78	15.65	6.15	–	38.72	–	0.74	–	–	–	19.5	99.55
		20.09	15.93	5.78	–	21.45	–	0.42	–	–	–	36.34	
Alloy of Pt-Fe-Au system	Pt-Fe-Au[1]	10.28	1.59	5.19	12.45	–	71.18	1.64	–	–	–	1.3	103.62
		23.69	3.49	10.51	8.14	–	46.97	1.98	–	–	–	5.22	
Laurite	RuS_2	1.04	0.66	1.26	–	–	–	0.59	44.51	16.77	0.88	34.54	100.26
		1.12	0.67	1.19	–	–	–	0.33	26.39	5.23	0.51	64.56	
		0.33	0.33	–	–	–	–	–	42.06	24.37	–	35.36	102.45
		0.36	0.34	–	–	–	–	–	25.11	7.65	–	66.55	
Cuproiridsite	CuIr2S4	3.58	2.98	8.01	–	–	3.26	–	–	56.44	2.40	24.09	100.75
		4.83	3.83	9.51	–	–	1.26	–	–	22.15	1.76	56.67	
Zone V (bnss+pnss)													
Cuproiridsite	CuIr2S4	3.57	2.84	7.99	–	–	4.71	–	–	54.87	2.73	23.63	100.35
		4.88	3.69	9.59	–	–	1.84	–	–	21.77	2.02	56.21	
Laurite	RuS2	0.34	0.37	–	–	0.21	–	0.14	45.13	18.85	0.46	35.40	100.88
		0.37	0.38	–	–	0.12	–	0.08	26.76	5.88	0.27	66.17	
		0.39	0.24	–	–	–	–	–	46.88	18.22	0.86	36.2	102.8
		0.41	0.24	–	–	–	–	–	27.17	5.55	0.49	66.14	
		0.28	0.39	–	–	–	–	–	42.93	22.4	1.19	35.5	102.69
		0.3	0.4	–	–	–	–	–	25.41	6.97	0.69	66.23	
		0.45	0.39	–	–	0.41	–	–	43.86	20.25	1.11	35.5	101.96
		0.48	0.4	–	–	0.23	–	–	25.89	6.29	0.64	66.07	
Native silver	Ag[1]	13.18	4.23	28.04	–	33.61	–	0.51	–	–	–	18.44	98.02
		14.38	4.39	26.89	–	18.99	–	0.29	–	–	–	35.05	
Gold-based alloy	Au*[1]	2.17	1.02	7.42	74.55	4.49	2.10	7.79	–	–	–	1.40	100.94
		5.39	2.41	16.20	52.51	5.78	1.49	10.16	–	–	–	6.06	
Pt-Fe-Au-ss	Pt-Fe-Au[1]	9.64	2.22	4.06	10.67	0.57	70.38	1.03	–	–	–	1.04	99.61
		23.43	5.13	8.67	7.35	0.72	48.97	1.31	–	–	–	4.4	
		9.22	2	4.09	13.1	0.39	70.13	1.41	–	–	–	1.18	101.53
		22.21	4.58	8.66	8.95	0.49	48.37	1.78	–	–	–	4.95	
		8.63	1.91	4.36	20.91	0.38	59.98	1.01	0	0	0	0.94	98.11
		21.72	4.57	9.64	14.92	0.5	43.2	1.33	0	0	0	4.12	
		Fe	Ni	Cu	Au	Ag	Pt	Pd	Ru	Ir	Rh	S	

Note. For each phase the composition expressed in wt. % is in the upper row, in at. % – in the lower row. ss- solid solution.

[1] – high content of major components indicates the entrapment of sulfide phases in the analyzed area of the matrix.

Ag. Native Ag was released in the form of rims less than 1 μm wide around bnss' and Ni-pn grains in zones IV and V of the sample. Elongated inclusions of Ag in the bnss' matrix were also observed there (Fig. 3k, m, p) (Table 5).

As can be seen from the above-described experimental results, micro-elements can be present as solid solutions in the primary and secondary main phases of the Fe–Ni–Cu–S system, as independent phases crystallized from the melt, or as a result of partial decomposition of sulfide solid solutions during their cooling, and also in the form of impurities dissolved in other microphases. Impurities of noble metals soluble in the main phases of this system distributed during crystallization in accordance with the classical theory, similar to macrocomponents. Thus, Ir and Ru dissolved well in the matrix of high-temperature mss, and upon cooling they transited into the low-temperature modification of mss'. Rhodium's behavior was more complex. It was present at the beginning of crystallization in mss, while the remaining Rh noticeably accumulated in the melt only in zone V, where it was present in pnss, upon decomposition of which in case of cooling it transited into Ni-mss. Palladium and silver were concentrated in the final products of melt crystallization, pentlandite and bornite solid solutions, respectively. The main low-temperature concentrator of Pd was pentlandite. A recent work [46] proved its inclusion in the pentlandite crystal lattice, and in [47] a discovery of pentlandite containing 11.26 wt. % Pd in Norilsk ores was reported.

Impurities that did not transit into sulfide solid solutions can form independent phases: primary ones directly in the process of fractional crystallization of the melt and secondary ones as a result of solid-phase reactions. It is likely that the compounds with a melting point significantly exceeding the crystallization temperature of this melt were formed from the melt. Crystallization of Pt_3Fe and mass formation of RuS_2 were associated with the initial stage of the directional crystallization process. Refractory RuS_2 (melting point ~ 1600 °C) was formed in the Ru-S binary system [44]. The Pt-Fe phase diagram contained a non-stoichiometric Pt_3Fe compound with a wide homogeneity region, formed as a result of the decomposition of a continuous solid solution at a temperature of 1350 °C ([48] and references from it).

It should be noted that Pt_3Fe inclusions were observed in the mss' matrix of zone I, while RuS_2 was found not only in this matrix, but also in the decomposition products of the eutectic alloys iss + bnss and bnss + pnss in zones IV and V, respectively, as an independent phase and in intergrowths with $CuIr_2S_4$. The formation of these phases directly from the melt was confirmed by the large sizes and expressed faceting of the inclusions. In accordance with the theory of quasi-equilibrium directional crystallization of multicomponent melts with impurities, the process of zoning formation made up by primary sulfide solid solutions should be accompanied by the formation of primary impurity zoning [49]. The impurity phases should appear in the ingot in a sequence, one after another. Each impurity zone was distinguished by its own set of microphases. The transition from one zone to another meant rather the disappearance or the emergence than the emergence of a new microphase. As a result, a regular change in the distribution of microphases should occur along the sample. In our experiment, this pattern was not observed. Thus, RuS_2 crystals were formed in zones I, IV, and V, which meant that there was no fractionation. It should be noted that the processes of formation of new phases upon directional crystallization were determined only by the processes of their incorporation at the crystallization front. Upon crystallization of phases composed of macrocomponents, a continuous crystallization front was formed. Upon crystallization of microphases, a continuous crystallization front could not be formed, and thus the main limiting stage was the formation of nuclei. The formation of nuclei occurred under strongly nonequilibrium conditions, and thus it was natural to expect that the theory of quasi-equilibrium directional crystallization would not work in this case.

Silver rims around secondary inclusions bnss' and Ni-pn were most likely formed as a result of solid-phase processes. Primary bnss partially captured Ag in the process of crystallization from the melt. In case of cooling, inclusions of Ag appeared due to a decrease in its solubility in bnss'. Secondary formations included Pt-Fe-Au solid solutions, which were observed to occur

within grains of secondary Ni-pn and Ni-mss, and this indicated their formation as a result of solid-phase reactions. They were represented by the structure of decomposition of Pt_3Fe and Au*. Au* inclusions were associated with iss' (hc) or with mh/Ni-mss boundaries. This suggested that their formation was a consequence of subsolidus iss decay. The processes of microphase separation during solid-phase reactions, as well as during crystallization from a melt, proceeded as nonequilibrium through the stage of nucleation and their subsequent growth.

4. Conclusions

In this work we obtained new data on the behavior of the main elements and impurities upon fractional crystallization of a multicomponent melt of the Cu-Fe-Ni-S-(PGE, Au, Ag) system with its own special type of zoning.

It was shown that during fractional crystallization the macrocomponents were distributed in accordance with the classical theory. Their behavior can be described using distribution coefficients. It was established that during melt crystallization, the sequence of primary phase formation had the following form: mss / mss + iss / iss / iss + bnss / bnss + pnss. These results indicated a more complex structure of the melting diagram in the studied region of the Fe-Ni-Cu-S system than was known before from classical experiments using samples obtained by long-term annealing and subsequent quenching.

The results of chemical analysis and the ingot microstructure study allowed determining a list of low-temperature secondary phases and their associations that must be taken into account when constructing subsolidus sections. A new type of secondary (phase) zonality may be present in Cu-Ni sulfide ores.

In the first approximation, the behavior of noble metal impurities upon fractional crystallization can be described using distribution coefficients. The processes of microphase separation from the melt or during solid-phase reactions proceeded as non-equilibrium through the stage of formation of nuclei and their subsequent growth. Therefore, the process of formation of impurity zonality did not strictly correspond to the theory of quasi-equilibrium directional crystallization of multicomponent melts with impurities.

Author contributions

E. F. Sinyakova: scientific supervision, methodology and concept development, research, writing of text, final conclusions. K. A. Kokh: methodology development, conducting experiments, research, text editing.

Conflict of interests

The authors declare that they have no known competing financial interests or personal relationships that could have influenced the work reported in this paper.

References

1. Craig J. R., Kullerud G. Phase relations in the Cu–Fe–Ni–S system and their application to magmatic ore deposits. *Economic Geology Monograph* / Ed. H.D.B. Wilson. 1969;4: 344–358. https://doi.org/10.5382/Mono.04.25

2. Fleet M. E., Chryssoulis S. L., Stone W. E., Weisener C. G. Partitioning of platinum-group elements and Au in the Fe–Ni–Cu–S system: experiments on the fractional crystallization of sulfide melt. *Contributions of Mineralogy and Petrology*. 1993;115: 36–44. https://doi.org/10.1007/BF00712976

3. Fleet M. E., Pan Y. Fractional crystallization of anhydrous sulfide liquid in the system Fe–Ni–Cu–S, with application to magmatic sulfide deposits. *Geochimica et Cosmochimica Acta*. 1994;58: 3369–3377. https://doi.org/10.1016/0016-7037(94)90092-2

4. Ebel D. S., Naldrett A. J. Crystallization of sulfide liquids and interpretation of ore composition. *Canadian Journal of Earth Sciences*. 1977;34: 352–356. https://doi.org/10.1139/e17-031

5. Дистлер В. В., Гроховская Т. Л., Евстигнеева Т. Л. и др. *Петрология сульфидного магматического рудообразования*. М.: Наука; 1988, 230 с.

6. Ballhaus C., Tredoux M., Spath A. Phase relations in the Fe-Ni-Cu-PGE-S system at magmatic temperature and application to massive sulphide ores of the Sudbery igneous complex. *Journal of Petrolology*. 2001;42(10): 1911–1926. https://doi.org/10.1093/petrology/42.10.1911

7. Naldrett A. J. *Magmatic sulfide deposits. Geology, geochemistry and exploration*. Springer-Verlag, Heidelberg, Germany; 2004, 727 p.

8. Fleet M. E. Phase equilibria at high temperature. *Reviews in Mineralogy and Geochemistry*. 2006;61: 365–419. https://doi.org/10.2138/rmg.2006.61.7

9. Cafagna F., Jugo P. J. An experimental study on the geochemical behavior of highly siderophile elements (HSE) and metalloids (As, Se, Sb, Te, Bi) in a mss-iss-pyrite system at 650 °C: a possible magmatic origin for Co-HSE-bearing pyrite and the role of metalloid-rich phases in the fractionation of HSE. *Geochimica et Cosmochimica Acta*. 2016;178: 233–258. https://doi.org/10.1016/j.gca.2015.12.035

10. Helmy H. M., Botcharnikov R., Ballhaus C., … Hager T. Evolution of magmatic sulfide liquids: how and when base metal sulfides crystallize? *Contributions of Mineralogy and Petrology*. 2021;176: 1–15. https://doi.org/10.1007/s00410-021-01868-4

11. Kullerud G., Yund R. A., Moh G. H. Phase relations in the Cu–Fe–S, Cu–Ni–S, and Fe–Ni–S systems. *Economic Geology Monograph*. 1969;4: 323–343.

12. Sugaki A., Kitakaze A. High form of pentlandite and its thermal stability. *American Mineralogist.* 1998;83(1–2): 133–140. https://doi.org/10.2138/am-1998-1-213

13. Cabri L. J. New phase relations in the Cu-Fe-S system. *Economic Geology*. 1973;68(4): 443–454. https://doi.org/10.2113/gsecongeo.68.4.443

14. Peregoedova A., Ohnenstetter M. Collectors of Pt, Pd and Rh in a S-poor Fe–Ni–Cu sulfide system at 760°C: experimental data and application to ore deposits. *The Canadian Mineralogist*. 2002;40: 527–561. https://doi.org/10.2113/gscanmin.40.2.527

15. Kosyakov V. I., Sinyakova E. F. Melt crystallization of $CuFe_2S_3$ in the Cu–Fe–S system. *Journal of Thermal Analysis and Calorimetry*. 2014;115(1): 511–516. https://doi.org/10.1007/s10973-013-3206-0

16. Sinyakova E. F., Vasilyeva I. G., Oreshonkov A. S., Goryainov S. V., Karmanov N. S. Formation of noble metal phases (Pt, Pd, Rh, Ru, Ir, Au, Ag) in the process of fractional crystallization of the $CuFeS_2$ melt. *Minerals*. 2022;12(9): 1136. https://doi.org/10.3390/min12091136

17. Tolstykh N., Brovchenko V., Rad'ko V., Shapovalova M., Abramova V., Garcia J. Rh, Ir and Ru partitioning in the Cu-poor IPGE massive ores, Talnakh intrusion, Skalisty mine, Russia. *Minerals*. 2022;11:18. https://doi.org/10.3390/min12010018

18. Mungall J. E. Crystallization of magmatic sulfides: an empirical model and application to Sudbury ores. *Geochimica et Cosmochimica Acta*. 2007;71(11): 2809–2819. https://doi.org/10.1016/j.gca.2007.03.026

19. Dare S. A. S., Barnes S.-J., Prichard H. M., Fisher P. C. Mineralogy and geochemistry of Cu-Rich ores from the McCreedy East Ni-Cu-PGE deposit (Sudbury, Canada): implications for the behavior of platinum group and chalcophile elements at the end of crystallization of a sulfide liquid. *Economic Geology*. 2014;109(2): 343–366. https://doi.org/10.2113/econgeo.109.2.343

20. Barnes S.-J., Ripley E. M. Highly siderophile and strongly chalcophile elements in magmatic ore deposits. *Reviews in Mineralogy and Geochemistry*. 2016;81: 725–774. https://doi.org/10.2138/rmg.2016.81.12

21. Duran, C. J., Barnes S. J., Plese P., Kudrna Prašek M., Zientek M. L., Pagé P. Fractional crystallization-induced variations in sulfides from the Noril'sk-Talnakh mining district (Polar Siberia, Russia). *Ore Geology Review*. 2017;90: 326–351. https://doi.org/10.1016/j.oregeorev.2017.05.016

22. Liu, Y., Brenan J., Partitioning of platinum-group elements (PGE) and chalcogens (Se, Te, As, Sb, Bi) between monosulfide-solid solution (MSS), intermediate solid solution (ISS) and sulfide liquid at controlled conditions. *Geochimica et Cosmochimica Acta*. 2015;159: 139–161. https://doi.org/10.1016/j.gca.2015.03.021

23. Hawley J. E. The Sudbury ores: their mineralogy and origin. *The Canadian Mineralogist*. 1962;7(1): 1–207.

24. Naldrett A. J., Ebel D. S., Asif M., Morrison G., Moore C. M. Fractional crystallization of sulfide melts as illustrated at Noril'sk and Sudbury. *European Journal of Mineralogy*. 1997;9: 365–377. https://doi.org/10.1127/ejm/9/2/0365

25. Barnes S-J., Cox R. A., Zientek M. L. Platinum-group element, gold, silver and base metal distribution in compositionally zoned sulfide droplets from the Medvezky Creek mine, Noril'sk, Russia. *Contributions of Mineralogy and Petrology*. 2006;152: 187–200. https://doi.org/10.1007/s00410-006-0100-9

26. Holwell D. A., McDonald I. A review of the behavior of platinum group elements within natural magmatic sulfide ore systems. *Platinum Metals Review*. 2010;54: 26–36. https://doi.org/10.1595/147106709x480913

27. Kosyakov V. I., Sinyakova E. F., Distler V. V. Experimental simulation of phase relationships and zoning of magmatic nickel–copper sulfide ores, Russia. *Geology of Ore Deposits*. 2012;54: 179–208. (In Russ., abstract in Eng.). https://doi.org/10.1134/S1075701512030051

28. Sinyakova E. F., Kosyakov V. I., Borisenko A. S., Karmanov N. S. Behavior of noble metals during fractional crystallization of Cu–Fe–Ni–(Pt, Pd, Rh, Ir, Ru, Ag, Au, Te) sulfide melts. *Russian Geology and Geophysics*. 2019; 60(6): 642–651. https://doi.org/10.15372/RGG2019050

29. Sinyakova E. F., Kosyakov V. I., Kokh K. A., Naumov E. A. Sequential crystallization of pyrrhotite, cubanite and intermediate solid solution from Cu-Fe-(Ni)-S melt. *Russian Geology and Geophysics*. 2019;60(11): 1257–1267. https://doi.org/10.15372/rgg2019091

30. Kosyakov V. I., Sinyakova E. F., Kokh K. A. Sequential crystallization of four phases from melt on the polythermal section of the Cu–Fe–Ni–S system. *Journal of Thermal Analysis and Calorimetry*. 2020;139(6): 3377–3382. https://doi.org/10.1007/s10973-019-08701-y

31. Kosyakov V. I., Sinyakova E. F. Physicochemical prerequisites for the formation of primary orebody zoning at copper-nickel sulfide deposits (by the example of the systemsFe–Ni–SandCu–Fe–S). *Russian Geology and Geophysics*. 2012;53(9): 861–882. https://doi.org/10.1016/j.rgg.2012.07.003

32. Kosyakov V. I. Possible usage of directional crystallization for solving petrological problems. *Russian Geology and Geophysics*. 1998;39(9): 1245–1256.

33. Sinyakova E. F., Kosyakov V. I. Experimental modeling of zonality of copper-rich sulfide ores in copper–nickel deposits. *Doklady Earth Sciences*. 2009;427: 787–792. https://doi.org/10.1134/S1028334X0709019X

34. Schlegel H., Sehüller A. Das Zustandebild Kupfer-Eisen-Schwefel. *Zeitschrift für Metallkunde*. 1952;43(12): 421–428.

35. Greig J. W., Jensen E., Merwin H. E. The system Cu-Fe-S. *Carnegie Institution of Washington Year Book*. 1955;54: 129–134.

36. Fleet M. E., Chryssoulis S. L., Stone W. E., Weisener C. G. Partitioning of platinum-group elements and Au in the Fe–Ni–Cu–S system: experiments on the fractional crystallization of sulfide melt. *Contributions of Mineralogy and Petrology*. 1993;115: 36–44. https://doi.org/10.1007/bf00712976

37. Li C., Barnes S.-J., Makovicky E. et al. Partitioning of nickel, cooper, iridium, rhenium, platinum, and palladium between monosulfide solid solution and sulfide liquid: Effects of composition and temperature. *Geochimica et Cosmochimica Acta*. 1996;60(7): 1231–1238. https://doi.org/10.1016/0016-7037(96)00009-9

38. Barnes S.-J., Makovicky E., Makovicky M., Rose-Hansen J., Karup-Moller S. Partition coefficients for Ni, Cu, Pd, Pt, Rh and Ir between monosulfide solid solution and sulfide liquid and the formation of compositionally zoned Ni-Cu sulphide bodies by fractional crystallization of sulfide liquid. *Canadian Journal of Earth Sciences*. 1997;34: 366–374. https://doi.org/10.1139/e17-032

39. Mungall J. E., Andrews D. R. A., Cabri L. J., Sylvester P. J., Tuberett M. Partitioning of Cu, Ni, Au, and platinum-group elements between monosulfide solid solution and sulfide melt under controlled oxygen and sulfur fugacities. *Geochimica et Cosmochimica Acta*. 2005;64(17): 4349–4360. https://doi.org/10.1016/j.gca.2004.11.025

40. Simon G., Kesler S. E., Essene E. J., Chryssoulis S. L. Gold in porphyry copper deposits: experimental determination of the distribution of gold in the Cu-Fe-S system at 400 to 700 °C. *Economic Geology*. 2000;95: 259–270. https://doi.org/10.2113/gsecongeo.95.2.259

41. Kolonin G. R., Fedorova Zh. N., Kravchenko T. A. Influence of the composition of phase associations of the Cu-Fe-S system on the mineral forms of rhodium (according to experimental data)*. *Doklady of the Academy of Sciences*. 1994;337(1): 104–107. (In Russ.)

42. Sinyakova E. F., Kosyakov V. I. Experimental modeling of zoning in copper-nickel sulfide ores. *Doklady Earth Sciences*. 2007;417A(9): 1380–1385. https://doi.org/10.1194/S1028334X0709019X

43. Sinyakova E. F., Komarov V. Yu, Sopov K. V., Kosyakov V. I., Kokh K. A. Crystallization of pyrrhotite from Fe-Ni-Cu-S-(Rh, Ru) melt. *Journal of Crystal Growth*. 2020;548: 125822. https://doi.org/10.1016/j.jcrysgro.2020.125822

44. Massalski T. B., Okamoto H., Subramanian P. R., Kacprzak L. *Binary Alloy Phase Diagrams. Second Edition*. Ohio, United States: ASM International, Materials Park; 1990. 3589 p.

45. Ternary alloy systems. Noble metal systems. Selected systems from Ag-Al-Zn to Rh-Ru-Sc. In: *Landolf-Börnstein – Group IV. Physical Chemistry*. G. Effenberg & S. Ilyenko (eds.). 2006;11B. https://doi.org/10.1007/b96200

46. Brovchenko V., Merkulova M., Sittner J., … Cnudde V. X-ray absorption spectroscopic study of Pd^{2+} on Ni site in pentlandite. *American Mineralogist*. 2023;108: 2086–2095. https://doi.org/10.2138/am-2022-8704

47. Kalugin V., Gusev V., Tolstykh N., Lavrenchuk A., Nigmatulina E. Origin of the Pd–rich pentlandite in the massive sulfide ores of the Talnakh deposit, Norilsk Region, Russia. *Minerals*. 2021;11(11): 1258. https://doi.org/10.3390/min11111258

48. Makovicky E. Ternary and quaternary phase systems with PGE. In*: The Geology, Geochemistry, Mineralogy and Mineral Beneficiation of Platinum-Group Elements*. L. J. Cabri (ed.) Canadian Institute of Mining. Metallurgy and Petroleum; 2002, Special Vol. 54, pp. 131-175.

49. Kosyakov V. I., Sinyakova E. F. Peculiarities of behavior of trace elements during fractional crystallization of sulfide magmas. *Doklady Earth Sciences*. 2015;460(2): 179–182. https://doi.org/10.1134/S1028334X1502021X

* *Translated by author of the article*

Information about the authors

Elena F. Sinyakova, Dr. Sci. (Geol.-Min.), Leading Research Fellow, V. S. Sobolev Institute of Geology and Mineralogy, Siberian Branch of the Russian Academy of Sciences (Novosibirsk, Russian Federation).

https://orcid.org/0000-0001-6288-3425

efsin@igm.nsc.ru

Konstantin A. Kokh, Dr. Sci. (Geol.-Min.), Leading Research Fellow, V. S. Sobolev Institute of Geology and Mineralogy, Siberian Branch of the Russian Academy of Sciences (Novosibirsk, Russian Federation).

https://orcid.org/0000-0003-1967-9642

kokh@igm.nsc.ru

Received 27.05.2024; approved after reviewing 31.05.2024; accepted for publication 16.09.2024; published online 25.12.2024.

Translated by Marina Strepetova